A Study on Trajectory Optimization for the Terminal Area

Daichi Toratani
Graduate School of Environment and Information Sciences
Yokohama National University
Yokohama, Japan
Toratani-daichi-jk@ynu.jp

Seiya Ueno
Research Institute of Environment and Information Sciences
Yokohama National University
Yokohama, Japan
s-ueno@ynu.ac.jp

***Abstract*—These days, congestion in the terminal area is getting worse. To resolve the problem, we study conflict resolution methods for the terminal area. To attain a conflict resolution method suitable for air traffic management, the BADA model was introduced to the optimal control theory. The unique coordinate system called the space-time coordinate system is applied to the trajectory optimization problem to attain a conflict resolution method suitable for the terminal area. In this paper, the optimal trajectory of climbing aircraft in the terminal area will be shown, and the conflict resolution method in the space-time coordinate system will be presented.**

Keywords-optimal control; BADA model; conflict resolution; terminal area

NOMENCLATURE

Thr	: Thrust [N]
D	: Aerodynamic drag [N]
V_{TAS}	: True airspeed [m/s]
m	: Aircraft mass [kg]
g_0	: Gravitational acceleration [m/s^2]
t	: Time [s]
γ	: Flight path angle [deg]
C_{Tc}	: Max. climb thrust coefficient (1: [N], 2: [ft], 3: [1/ft^2])
H_p	: Pressure altitude [m]
C_D	: Drag coefficient
ρ_a	: Atmospheric density [kg/m^3]
S	: Wing reference area [m^2]
C_L	: Lift coefficient
ϕ	: Bank angle [deg]
p_0	: Standard atmospheric pressure at MSL [N/m^2]
R	: Real gas constant for air [m^2/(K·s^2)]
T_0	: Standard atmospheric temperature at MSL [K]
β	: ISA temperature gradient with altitude below the tropopause [K/m]
ψ	: Azimuth angle [deg]
p	: Rate of change of the flight path angle [deg/s]
f_{nom}	: Nominal fuel flow [kg/s]
C_f	: Thrust specific fuel consumption coefficient (1: [kg/(s·N)], 2: [kt])
X	: State vector
U	: Input vector
ϕ_d	: Dummy input for bank angle [deg]
J	: Criterion
L	: Objective function
w	: Weight
H	: Hamiltonian
λ, ρ, ν	: Adjoint vector
Ω	: Terminal condition of state variable
N	: Division number of trajectory
s	: Length of trajectory in space-time coordinate system
f_{total}	: Total fuel consumption [kg]
κ	: Curvature of trajectory [1/m]
r	: Semi-axis of ellipsoid
B	: Barrier function
r_b	: Coefficient of barrier function
C_{st}	: Space-time coefficient
d	: Minimum distance [m]
$t_{sep.}$	: Minimum time separation [s]

ACCENT AND SUBSCRIPT

$\sim$	: Dimensionless parameter
$_0$	: Initial
$_f$	: Terminal
$_s$	: Spatial
$_t$	: Temporal
$_{ref.}$	: Reference
$_e$	: Center of ellipsoid

I. INTRODUCTION

World air-passenger traffic is growing steadily. Along with this growth, civil aviation has increasing problems, for example, fuel reduction, CO2 emission reduction, and noise pollution. Especially, congestion in the terminal area: the airspace near the airport, is a serious problem. From this congestion, the air traffic controller (ATC) workload is increasing, and delays of arrival aircraft occur. The risk of collision increases in such conditions. Therefore, conflict-free trajectory generation methods in the terminal area is required.

One of the most efficient approaches for generating conflict-free trajectory is an optimal control approach. There are many previous attempts with respect to conflict-free trajectory

optimization for aircraft using the optimal control theory [1, 2], but they are not suitable for commercial aircraft. That is why the commercial aircraft model is not employed in these studies. In the field of air traffic management (ATM), the base of aircraft data (BADA) model is widely used. The BADA model is composed of some equations and datasets based on real commercial aircraft developed by EUROCONTROL [3], and the model is widely used for the simulation and validation of new ATM concepts [4, 5]. There is some previous research with respect to trajectory optimization using the BADA model [6]. However, there are a few researches about conflict-free trajectory optimization suitable for the ATM.

The target of this study is to attain the conflict-free trajectory optimization methods in the terminal area. First, the trajectory optimization for single aircraft using the BADA is used to attain the trajectory optimization methods suitable for ATM. Second, a unique coordinate system is introduced to the optimization problem as shown in Fig. 1. This coordinate system is called the space-time coordinate system [7, 8]. In this coordinate system, the vertical axis is time, and time and velocity are able to be treated along with position and angle. By using this coordinate system, it becomes easier to express conflict resolution in the terminal area. For example, the aircraft in the terminal area resolve conflict by vectoring and changing their velocity. In this paper, they are called the spatial conflict resolution and the temporal conflict resolution. Using the space-time coordinate system, both conflict resolutions are able to be treated in a similar way, and they are able to be optimized simultaneously.

This paper is composed of 3 chapters followed by the summaries and the future plans for this study. Chapter 2 presents trajectory optimization using the time-independent coordinate system. Chapter 3 presents trajectory optimization in the space-time coordinate system. In these chapters, the models of the aircraft's trajectory, the optimization method, and optimization results are expressed respectively.

II. Trajectory Optimization for Time-Independent Coordinate System

This chapter presents a trajectory optimization method where the independent variable is time. In this study, the optimal control theory is applied to optimize the trajectory of the aircraft. The optimal control problem based on the Euler-Lagrange equation is formulated, and the solving method for the optimal control problem is expressed.

A. Aircraft Model

The model of the aircraft is based on the BADA model. Especially, the model is formulated to be suitable for climbing aircraft in the terminal area in this paper. In the BADA model, the vertical model of the aircraft is expressed as

$$(Thr - D)V_{TAS} = mg_0\frac{dh}{dt} + mV_{TAS}\frac{dV_{TAS}}{dt}. \quad (1)$$

Equation (1) is called the total-energy model (TEM) and equates the rate of work done by forces acting on the aircraft to the rate of increase in potential and kinematic energy. Defining the flight pass angle of the aircraft γ, equation (1) is transformed to as

$$m\frac{dV_{TAS}}{dt} = Thr - D - mg\sin\gamma. \quad (2)$$

Here, the thrust is expressed as

$$Thr = C_{Tc,1}\left(1 - \frac{H_p}{C_{Tc,2}} + C_{Tc,3}H_p^2\right). \quad (3)$$

This equation is defined as maximum climb and take-off thrust by the BADA. The drag is expressed as

$$D = \frac{C_D\rho_a V_{TAS}^2 S}{2}, \quad (4)$$

where the drag coefficient is derived as

$$\begin{aligned} C_D &= C_{D0} + C_{D2}C_L^2 \\ &= C_{D0} + C_{D2}\left(\frac{2mg}{\rho_a V_{TAS}^2 S\cos^2\phi}\right)^2. \end{aligned} \quad (5)$$

The atmospheric density is defined as a function of the altitude as

$$\rho_a = \frac{p_0}{RT_0}\left(1 + \frac{\beta}{T_0}H_p\right)^{-1-\frac{g}{\beta R}}. \quad (6)$$

This study focuses on the terminal area, and the atmospheric model and data below the tropopause are used. The rate of turn of the aircraft is calculated as a function of the bank angle as

$$\frac{d\psi}{dt} = \frac{g_0}{V_{TAS}}\tan\phi. \quad (7)$$

Here, the roll angle of the aircraft ϕ is constrained as

$$|\phi| \le \phi_{max}. \quad (8)$$

In Fig. 2, the position of the aircraft is formulated as

$$\frac{d}{dt}\begin{pmatrix} x \\ y \\ H_p \end{pmatrix} = \begin{pmatrix} V_{TAS}\cos\gamma\cos\psi \\ V_{TAS}\cos\gamma\sin\psi \\ V_{TAS}\sin\gamma \end{pmatrix}. \quad (9)$$

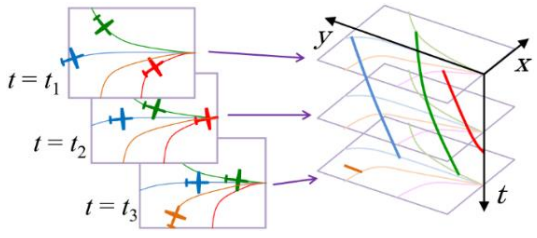

Figure 1. Schematic image of the space-time coordinate system.

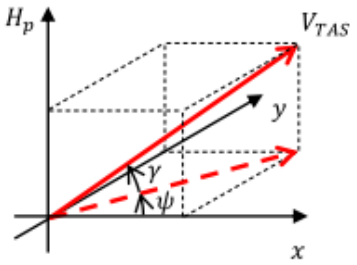

Figure 2. Relationship between velocity and position.

Therefore, the equation of motion for the aircraft is derived as

$$\frac{d}{dt}\begin{pmatrix}\psi\\ V_{TAS}\\ \gamma\\ x\\ y\\ H_p\end{pmatrix}=\begin{pmatrix}\frac{g}{V_{TAS}}\tan\phi\\ Thr-D-mg\sin\gamma\\ p\\ V_{TAS}\cos\gamma\cos\psi\\ V_{TAS}\cos\gamma\sin\psi\\ V_{TAS}\sin\gamma\end{pmatrix}, \tag{10}$$

by (2), (7) and (9). In this equation, the input values are ϕ and p. The nominal fuel flow is calculated as

$$f_{nom}=C_{f1}\left(1-\frac{V_{TAS}}{C_{f2}}\right)Thr. \tag{11}$$

The optimal control problem is formulated by using (10) as a constraint equation and (11) as a criterion.

B. Optimal Control Problem Formulation

To formulate the optimal control problem, the state variable and the input variable are defined in (12) and (13).

$$X=(\psi \quad V_{TAS} \quad \gamma \quad x \quad y \quad H_p)^T, \tag{12}$$

$$U=(\phi \quad \psi)^T, \tag{13}$$

To formulate the optimal control problem as a free terminal time problem, (10) is transformed to

$$\frac{dX}{d\tilde{t}}=\begin{pmatrix}t_f\frac{g}{V_{TAS}}\tan\phi\\ t_f(Thr-D-mg\sin\gamma)\\ t_f p\\ t_f V_{TAS}\cos\gamma\cos\psi\\ t_f V_{TAS}\cos\gamma\sin\psi\\ t_f V_{TAS}\sin\gamma\end{pmatrix}, \tag{14}$$

The constraint for the input as shown in (8) is transformed to

$$C=\phi-\phi_{max.}\sin\phi_d=0, \tag{15}$$

to transform the inequality constraint to the equality constraint. The criterion of the problem to minimize, is formulated as

$$J=\int_{t_0}^{t_f}L\,d\tilde{t}, \tag{16}$$

where L is defined as (17)

$$L=\frac{w_\phi}{2}\phi^2+\frac{w_p}{2}p^2+w_{ff}f_{nom}, \tag{17}$$

to minimize the inputs and the fuel consumption. In this paper, the problem is formulated for the free terminal time problem, and the terminal V_{TAS} and γ are free. The necessary conditions for the optimal control problem are derived as shown (18) to (25) [9].

$$\dot{X}=F(X,U,t), \tag{18}$$

$$H=L+\lambda^T F+\rho^T C, \tag{19}$$

$$\dot{\lambda}=-\left(\frac{\partial H}{\partial X}\right)^T, \tag{20}$$

$$\frac{\partial H}{\partial U}=0, \tag{21}$$

$$\Omega(X,t)|_{\tilde{t}=t_f}=\begin{pmatrix}\psi_h-\psi_{hf}\\ x-x_f\\ y-y_f\\ H_{ph}-H_{pf}\end{pmatrix}\Bigg|_{\tilde{t}=t_f}=0, \tag{22}$$

$$G=\nu^T\Omega, \tag{23}$$

$$\lambda(t_f)=\left(\frac{\partial G}{\partial X}\right)^T\Bigg|_{\tilde{t}=t_f}, \tag{24}$$

$$\left(\frac{\partial G}{\partial \tilde{t}}+H\right)\Big|_{\tilde{t}=t_f}=0. \tag{25}$$

Therefore, the optimal control problem is transformed to a two-point boundary value problem (TPBVP) by the differential equations (18) and (20), the constraint equations (15), (21) and (25), and the boundary conditions (22) and (24).

C. Optimization Method

To solve the TPBVP formulated in the previous section, the state variable and differential equations are discretized as

$$X_k=X(k/N)(k=0,\cdots,N), \tag{26}$$

$$2N(X_{k+1}-X_k)=F(X_{k+1})+F(X_k), \quad (k=0,\cdots,N-1). \tag{27}$$

In a similar way, the constraint equation (21) is discretized as

$$\frac{\partial H}{\partial U}(X_k,U_k,\lambda_k)=0 \ \ (k=0,\cdots,N). \tag{28}$$

From the discretization, the TPBVP is transformed to nonlinear simultaneous equations. The equations are solved by using the fsolve function in the Optimization Toolbox of the MATLAB. The fsolve is a useful solution system for nonlinear equations.

D. Optimization Result

The optimal control problem was solved under the conditions as table I. As previously mentioned, the terminal V_{TAS} and γ are free, and the terminal ψ_f, x_f, y_f and H_{pf} are specified. In this problem, the Boeing 777-200 is employed to calculate the optimal trajectory, and the constants with respect to the aircraft parameters and the atmosphere are taken from the BADA. Fig. 3 and 4 show the optimal trajectory in the three-dimensional space and the x-y plane respectively. In these figures, the initial and the terminal positions of the aircraft are indicated by the circle and the triangle markers. Fig. 5 to 11 are the time history of the azimuth angle, the true airspeed, the flight path angle, the pressure altitude, the rate of change of the flight path angle and the nominal fuel flow of the optimization results. Fig. 3 shows that the optimal trajectory in the terminal area is obtained by solving the optimal control problem. Fig. 4 shows that the minimum fuel trajectory is a rectilinear trajectory rather than a gradual trajectory as a circular arc. That is why the fuel

consumption critically depends on the flight time, and the shortest trajectory is optimal. Therefore, in Fig. 5 and 9, the bank angle reaches the limit value to turn with the maximum rate of turn at the initial and the terminal times. Fig. 7 and 8 show the aircraft climbs as quickly as possible. It seems that the fuel consumption is lower at higher altitudes. That is why the atmospheric density is lower at higher altitudes in (6), and the aerodynamic drag is lower at higher altitudes. This behavior is known as “higher for longer” in the field of ATM [10]. The optimization results are derived as table II.

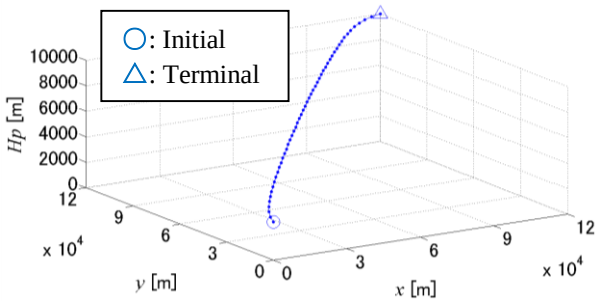

Figure 3. Optimal trajectory in the three-dimensional space.

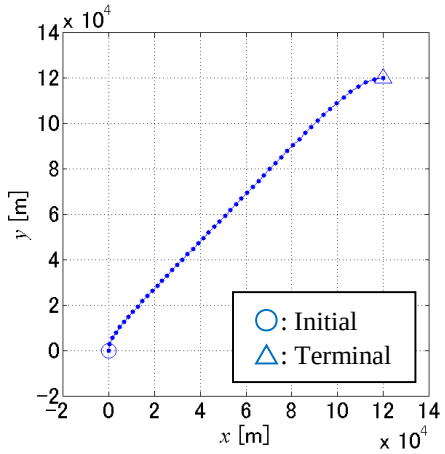

Figure 4. Optimal trajectory in the x-y plane.

TABLE I. Calculation conditions.

	Parameter	Value	Unit
Division number	N	50	[-]
Initial azimuth angle	ψ_0	90	[deg]
Initial true airspeed	V_{TAS0}	200	[m/s]
Initial flight path angle	γ_0	5	[deg]
Initial position	x_0	0	[m]
	y_0	0	[m]
	H_{p0}	3000	[m]
Terminal azimuth angle	ψ_f	0	[deg]
Terminal position	x_f	120000	[m]
	y_f	120000	[m]
	H_{pf}	10000	[m]

TABLE II. Optimization results.

	Parameter	Value	Unit
Terminal time	t_f	717.08	[s]
Terminal true airspeed	V_{TASf}	274.45	[deg]
Terminal flight path angle	γ_f	1.00	[deg]
Total fuel consumption	f_{total}	2647.41	[kg]

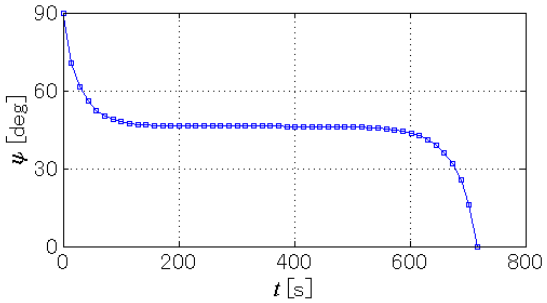

Figure 5. Time history of the azimuth angle.

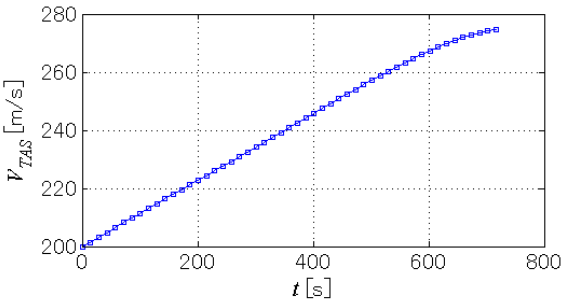

Figure 6. Time history of the true airspeed.

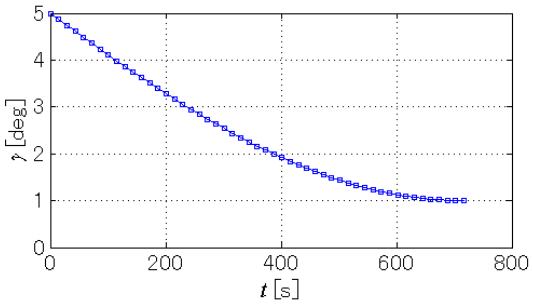

Figure 7. Time history of the flight path angle.

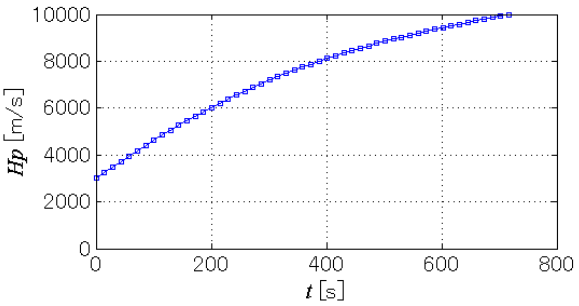

Figure 8. Time history of the pressure altitude.

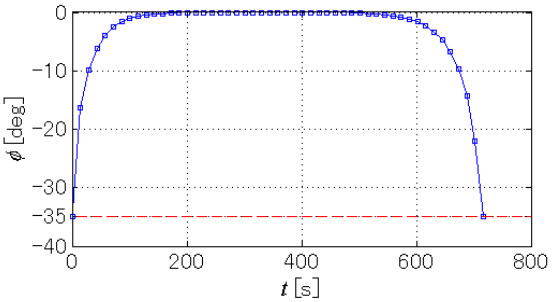

Figure 9. Time history of the bank angle.

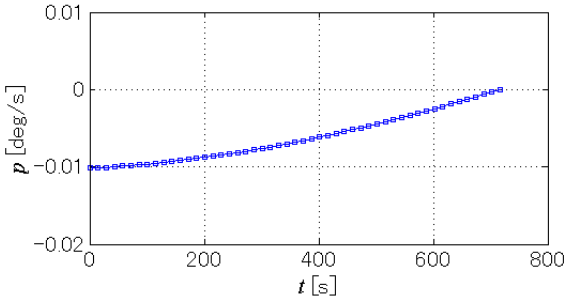

Figure 10. Time history of the rate of change of the flight path angle.

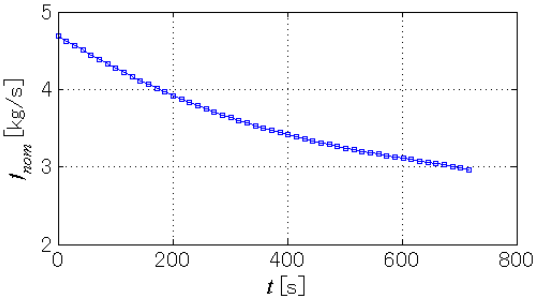

Figure 11. Time history of the nominal fuel flow.

III. Trajectory Optimization for the Space-Time Coordinate System

This chapter presents the conflict resolution method in the space-time coordinate system. To calculate the conflict-free trajectory, the result obtained by the previous chapter is used. The conflict resolution method suitable for the terminal area is attained by using the unique coordinate system called the space-time coordinate system. In this paper, the simple conflict resolution method is presented using the prohibited area expressed by the barrier function.

A. Trajectory Model in the Space-Time Coodinate System

The aircraft trajectory model in the space-time coordinate system is defined as shown Fig. 12. In this coordinate system, the vertical axis is time, and the independent variable of the system is the length of the trajectory s. In the space-time coordinate system, conflict resolution using both vectoring and changing velocity are able to be calculated in same framework. In Fig. 12, the velocity of aircraft is derived as

$$V = \frac{dl}{dt} = \frac{1}{\tan\psi_t}. \tag{29}$$

In the space-time coordinate system, the state equation relating to time is derived as

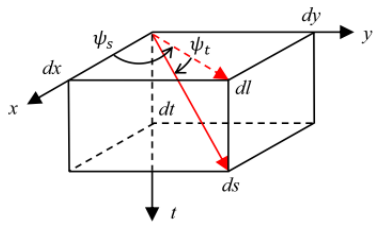

Figure 12. Definition of the space-time coordinate system.

$$\frac{dt}{ds} = \sin\psi_t. \tag{30}$$

By Fig. 12 and (30), the state equation of the aircraft trajectory model in the space-time coordinate system is expressed as

$$\frac{d}{ds}\begin{pmatrix}\psi_s\\ \psi_t\\ x\\ y\\ t\end{pmatrix} = \begin{pmatrix}\kappa_s\\ \kappa_t\\ \cos\psi_t\cos\psi_s\\ \cos\psi_t\sin\psi_s\\ \sin\psi_t\end{pmatrix}, \tag{31}$$

where κ are ψ differentiated by s (i.e., the curvatures of the trajectory), and κ are inputs to the state equation. In this paper, the azimuth angle in the space-time coordinate system ψ_s is called the spatial angle, and the elevation angle ψ_t is called the temporal angle. The same applies to the curvatures: κ_s and κ_t, are called the spatial and the temporal curvatures respectively.

B. Optimization Method

In the previous section, the state equations of the aircraft trajectory is formulated, but the equations do not include the vertical dynamics model of the aircraft as the TEM. To reflect the vertical dynamics, the optimization result obtained by the chapter 2 is applied, and the objective function for the criterion is defined as

$$\begin{aligned} L = {} & \frac{w_{\kappa_s}}{2}{\kappa_s}^2 + \frac{w_{\kappa_t}}{2}{\kappa_t}^2 \\ & + \frac{w_{\psi_s}}{2}\left(\psi_s - \psi_{sref.}\right)^2 + \frac{w_{\psi_t}}{2}\left(\psi_t - \psi_{tref.}\right)^2, \end{aligned} \tag{32}$$

where the first and second terms minimize the inputs, and third and fourth terms are employed to follow the optimal trajectory obtained by the chapter 2. To introduce conflict resolution, the inequality constraint is introduced as

$$g = -\left(\frac{x-x_e}{r_s}\right)^2 - \left(\frac{y-y_e}{r_s}\right)^2 - \left(\frac{t-t_e}{r_t}\right)^2 + 1 \le 0. \tag{33}$$

Equation (33) expresses a prohibited area and time to fly as an ellipsoid in the space-time coordinate system. To introduce the inequality constraint to the optimal control problem, (33) is transformed as

$$B = \frac{1}{g^2}. \tag{34}$$

Equation (34) is a barrier function as shown Fig. 13. This function increases to infinity near the boundary of the feasible region [11]. Expanding the objective function as (35), the

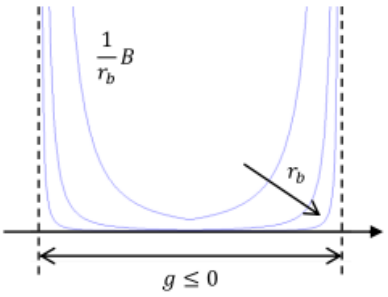

Figure 13. Schematic image of the barrier function.

criterion minimized by the optimization problem increases dramatically if the calculated solution violates the inequality constraint.

$$L' = L + \frac{1}{r_b}B. \tag{35}$$

The necessary conditions of the optimal control problem are derived in the similar way of the chapter 2. In this problem, the terminal length is free, and the terminal ψ_t and t are free. The derived TPBVP is discretized along with the chapter 2, and the nonlinear equations are solved using fsolve of MATLAB.

C. Optimizatin Result without Conflict

Before expressing the result of conflict resolution, the optimization result without conflict in the space-time coordinate system is shown. The optimal control problem is solved under the conditions as table III. In the space-time coordinate system, the temporal angle corresponds to the true airspeed, and the initial temporal angle ψ_{t0} is derived by (29). In table III, 0.28 [deg] is equal to 200 [m/s] along with the reference trajectory. The weights are determined the calculated trajectory to be able to follow the reference trajectory, and the weights are used for the conflict resolution that is shown later. Fig. 14 and 15 show the optimal trajectories in the space-time coordinate system and the x-y plane respectively. In these figures, the blue line shows the optimal trajectory, and the red line shows the reference trajectory obtained in the chapter 2. Fig. 16 to 18 are the time history of the spatial angle, the temporal angle, and the true airspeed. Basically, the independent variable is the length of the trajectory in the space-time coordinate system, but the horizontal axes of these figures are time for ease to see motion of the aircraft. By Fig. 14 and 15, it is confirmed that the optimal trajectory without conflict is able to follow the reference trajectory. Moreover, the spatial and the temporal angles are also able to follow the reference angles in Fig. 16 and 17. Fig. 18 is derived by using (29). The optimization results are derived as table IV.

D. Optimization Result with Conflict Resolution

In this section, the optimization results with conflict resolution in the space-time coordinate system are shown. Aircraft in the terminal area resolve conflict using vectoring or changing their velocity. In this paper, the conflict resolution with vectoring is called the spatial conflict resolution, and the conflict resolution changing velocity is called the temporal conflict

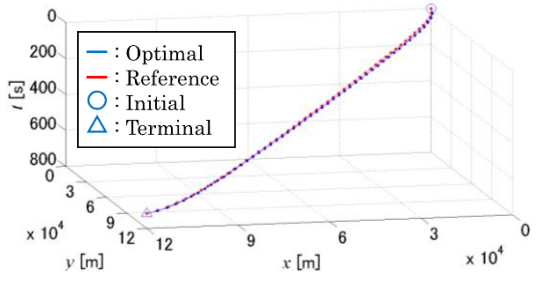

Figure 14. Optimal trajectory without conflict in the space-time coordinate system.

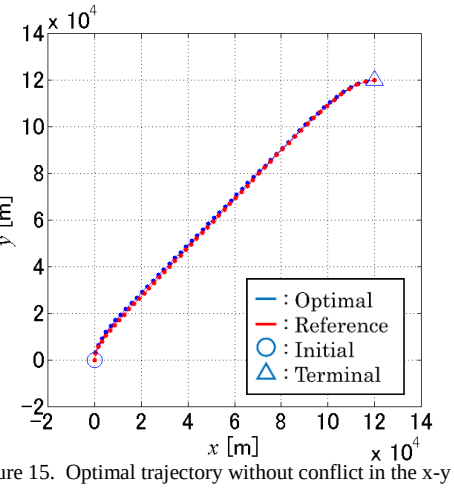

Figure 15. Optimal trajectory without conflict in the x-y plane.

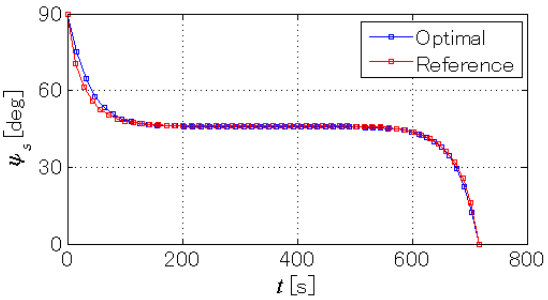

Figure 16. Time history of the spatial angle without conflict.

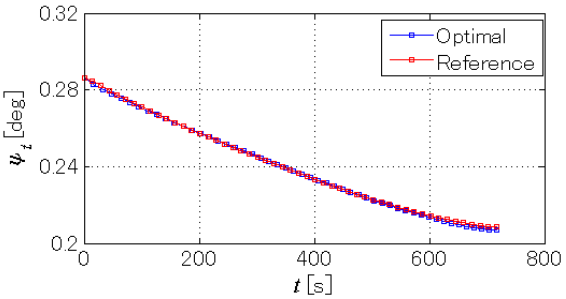

Figure 17. Time history of the temporal angle without conflict.

TABLE III. Calculation conditions.

	Parameter	Value	Unit
Division number	N	50	[-]
Initial spatial angle	ψ_{s0}	90	[deg]
Initial temporal angle	ψ_{t0}	0.29	[deg]
Initial position	x_0	0	[m]
	y_0	0	[m]
Initial time	t_0	0	[s]
Terminal spatial angle	ψ_{sf}	0	[deg]
Terminal position	x_f	120000	[m]
	y_f	120000	[m]
Weight for spatial curvature	w_{κ_s}	0.01	[-]
Weight for temporal curvature	w_{κ_t}	0.05	[-]
Weight for spatial angle	w_{ψ_s}	10	[-]
Weight for temporal angle	w_{ψ_t}	100	[-]

TABLE IV. Optimization results.

	Parameter	Value	Unit
Terminal temporal angle	ψ_{tf}	0.21	[deg]
Terminal time	t_f	717.08	[s]

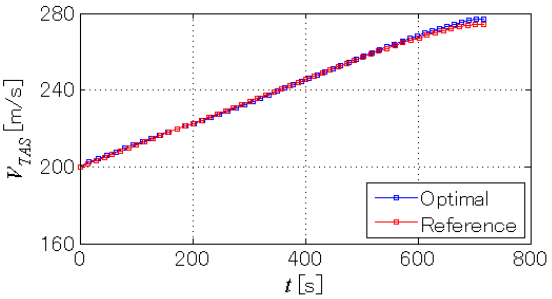

Figure 18. Time history of the true airspeed.

resolution. It depends on the weights for the spatial and the temporal angle which conflict resolutions are employed. To specify it, the weights for the spatial and the temporal angle are expanded as

$$w'_{\psi_s} = C_{st} w_{\psi_s}, \tag{36}$$

$$w'_{\psi_t} = \frac{1}{C_{st}} w_{\psi_t}, \tag{37}$$

where the space-time coefficient C_{st} is specified arbitrarily. For example, C_{st} is equal to 2, the weight for the spatial angle w_{ψ_s} is doubled, and the weight for the temporal angle w_{ψ_t} is multiplied by one-half. Then the weight for the spatial angle is larger than the weight for the temporal angle, and the deviation of the spatial angle is more minimized than the deviation of the temporal angle. Accordingly, the temporal conflict resolution is employed. Fig. 19 and 20 show the optimal trajectories with the spatial and temporal conflict resolution in the space-time coordinate system. To obtain both conflict resolutions, the space-time coefficient is specified as table V. In these figures, the blue line shows the trajectory with the spatial and the temporal conflict resolution, the red line shows the trajectory without conflict, and the ellipsoid is the prohibited area. In this problem, the parameters of the ellipsoid is set as table VI. The center of the ellipsoid is determined corresponding to the center of the trajectory of the case without conflict. The semi-axes of the ellipsoid are determined as 5 percent of the terminal position and the time. Fig. 21, 22 and 23 show the time history of the spatial angle, the temporal angle, and the true airspeed. In these figures, the blue line shows the case without conflict, the red line shows the case with the spatial conflict resolution, and the green line shows the case with the temporal conflict resolution. The optimization results are shown table VII. By Fig. 19 and 20, it is confirmed that both conflict resolutions are able to resolve the conflict with the ellipsoid. However, it is not clear to see the conflict resolution. To see clearly, Fig. 24 shows the optimal trajectories in x-y plane, and Fig. 25 shows the optimal trajectories viewed from the bottom right of Fig. 24. In Fig. 24 and 25, the minimum distance and the minimum time separation points between aircraft and the prohibited area are indicated by the square mark. The minimum distance and the minimum time separation between aircraft and the prohibited area, are shown in table VIII. Fig. 24 shows that the trajectory with the spatial conflict resolution resolves the conflict taking roundabout path. By contrast, the trajectory with the temporal conflict resolution resolves the conflict changing its velocity in Fig. 25. These features are also confirmed by Fig. 21 and 23. In Fig. 21, the

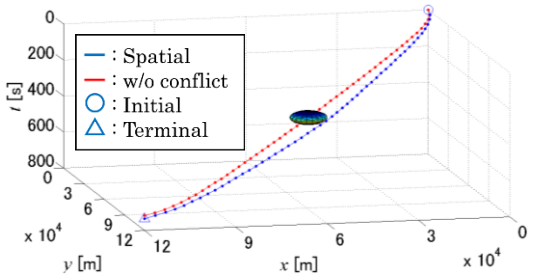

Figure 19. Optimal trajectory with the spatial conflict resolution in the space-time coordinate system.

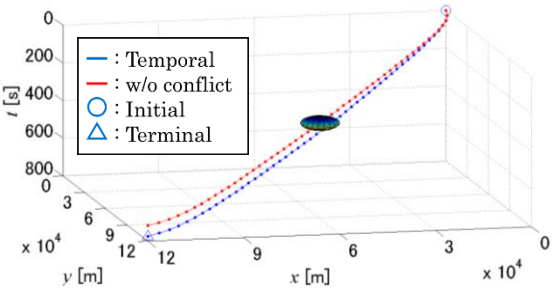

Figure 20. Optimal trajectory with the temporal conflict resolution in the space-time coordinate system.

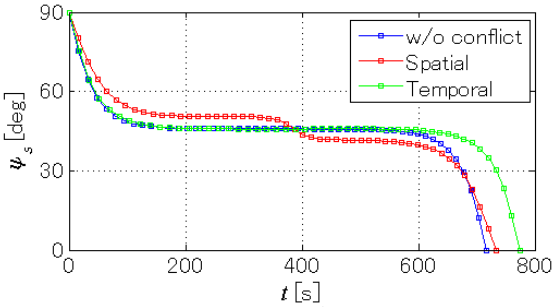

Figure 21. Time history of the spatial angle.

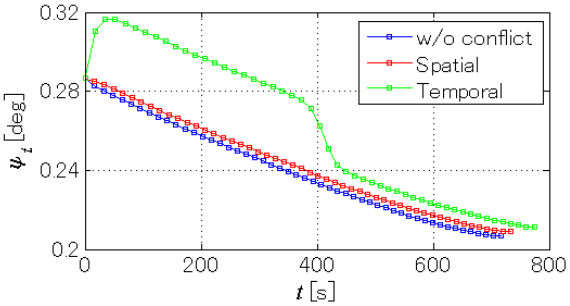

Figure 22. Time history of the temporal angle.

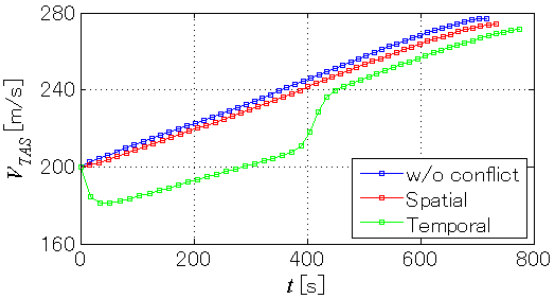

Figure 23. Time history of the true airspeed.

TABLE V. Weights for conflict resolution.

Spatial conflict resolution	C_{st}	1/2
Temporal conflict resolution	C_{st}	2

TABLE VI. Parameters of the ellipsoid of the prohibited area.

	Parameter	Value	Unit
Center of ellipsoid	x_e	53575.53	[m]
	y_e	63336.39	[m]
	t_e	378.76	[t]
Semi-axis of ellipsoid	r_s	6000	[m]
	r_t	35.85	[t]
Coefficient of barrier function	r_b	100	[-]

TABLE VII. Optimization results.

Spatial conflict resolution	Parameter	Value	Unit
Terminal temporal angle	ψ_{tf}	0.21	[deg]
Terminal time	t_f	732.97	[s]
Temporal conflict resolution	Parameter	Value	Unit
Terminal temporal angle	ψ_{tf}	0.21	[deg]
Terminal time	t_f	774.14	[s]

TABLE VIII. Result of conflict resolution.

Spatial conflict resolution	Parameter	Value	Unit
Minimum distance	d	833.84	[m]
Temporal conflict resolution	Parameter	Value	Unit
Minimum separation time	$t_{sep.}$	5.58	[s]

spatial conflict resolution is different from the case without conflict, and the temporal conflict resolution is similar to the case without conflict. Namely, the spatial conflict resolution mainly uses the spatial control to resolve conflict. In Fig. 23, the true airspeed of the spatial conflict resolution is similar to the case without conflict. By contrast, the temporal conflict resolution deviates from the case without conflict. By the results, it is confirmed that the conflict resolution method in the space-time coordinate system is derived. Moreover, both spatial and temporal conflict resolutions are able to be calculated in same framework by using the space-time coordinate system.

IV. Summaries and Future Plans

The trajectory optimization method in the terminal area is shown. The BADA is applied as the aircraft model to the optimal control theory. The optimal control problem for the terminal area is formulated based on the optimal control theory. The optimal climbing trajectory is obtained. The conflict resolution method suitable for the terminal area is also shown. To attain the conflict resolution method, the unique coordinate system called the space-time coordinate system is employed. The vertical axis of the space-time coordinate system is time, and velocity is expressed as an angle in the space-time coordinate system. The spatial and the temporal conflict resolutions are derived by same framework using the space-time coordinate system.

The future plans on this study is to improve the conflict resolution method. In this paper, the simple conflict resolution using barrier function is employed. In the next step, conflict resolution between two aircraft in the space-time coordinate system will be shown.

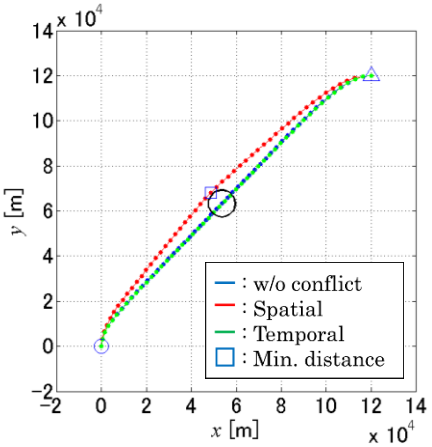

Figure 24. Optimal trajectory in the x-y plane.

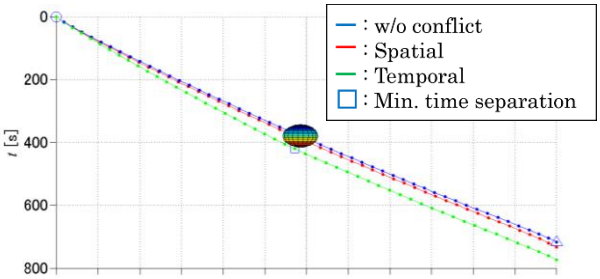

Figure 25. Optimal trajectory viewed from the bottom right of Fig. 24.

References

[1] J. Hu, M. Prandini, and S. Sastry, "Optimal coordinated maneuvers for three-dimensional aircraft conflict resolution," Journal of Guidance, Control, and Dynamics, Vol. 25, No. 5, pp. 888-900, 2002.

[2] A. Bicchi, and L. Pallottino, "On optimal cooperative conflict resolution for air traffic management systems", IEEE Transactions on Intelligent Transportation Systems, Vol. 1, Issue 4, pp. 221-231, 2000.

[3] EUROCONTROL, "User manual for the base of aircraft data (BADA) revision 3.10", EEC Technical/Scientific Report No. 12/04/10-45.

[4] A. Harada, Y. Miyamoto, Y. Miyazawa, and K. Funabiki, "Accuracy evaluation of an aircraft performance model with airliner flight data", Transactions of the JSASS, Aerospace Technology Japan, Vol. 11, pp. 79-85, 2013.

[5] K. Roach, and J. E. Robinson III, "A terminal area analysis of continuous ascent departure fuel use at Dallas/Fort Worth international airport", Proceedings of the 10th AIAA Aviation Technology, Integration, and Operations (ATIO) Conference, 2010.

[6] Y. Miyamoto, N. K. Wickramasinghe, A. Harada, Y. Miyazawa, and K. Funabiki, "Analysis of fuel-efficient airliner flight via dynamic programming trajectory optimization", Transactions of the JSASS, Aerospace Technology Japan, Vol. 11, pp. 93-98, 2013.

[7] D. Toratani, S. Ueno, and T. Higuchi, "Study on optimal conflict-free trajectory for air traffic management in terminal area", Proceedings of the Asia-Pasific International Symposium on Aerospace Technology, 01-10-3, 2013.

[8] J. Hu, M. Prandini, and S. Sastry, "Optimal maneuver for multiple aircraft conflict resolution: a braid point of view", Proceedings of the 39th IEEE Conference on Decision and Control, Vol. 4, pp. 4154-4169, 2000.

[9] E. Bryson, and Y. C. Ho, Applied optimal control: Optimization, Estimation, and Control, Taylor & Francis Group, pp. 42-89, 1975.

[10] A. Andreeva-Mori, S. Suzuki, and E. Itoh, "Scheduling of arrival aircraft based on minimum fuel burn descents", ASEAN Engineering Journal, 2011.

[11] T. Ohtsuka, Introduction to nonlinear optimal control, Corona Publishing CO., LTD., pp. 47-51, 2011.